

Adsorption and Corrosion Inhibition Behaviour of Oil Extracted from *Moringa peregrina* leaves for Carbon Steel in Acidic Media: Experimental and Computational Studies

Ismat H. Ali^{1,*}, Mohammad I. Khan², Alhafez M. Alraih^{3,4}, Mohammed K. Almesfer², Abubakr Elkhaleefa², Saif M. Dmour⁵, Mohammad Rehan⁶

¹ Department of Chemistry, College of Science, King Khalid University, P. O. Box 9004, Postal Code 61413, Abha, Kingdom of Saudi Arabia

² Department of Chemical Engineering, College of Engineering, King Khalid University, Abha, Kingdom of Saudi Arabia

³ Department of Chemistry, College of Science and Arts, King Khalid University, Kingdom of Saudi Arabia

⁴ Department of Chemistry, Faculty of Education, Gezira University, Sudan

⁵ Department of Medical Analysis, Princess Aisha Bint Al-Hussein, Faculty of Nursing and Health Sciences, Al-Hussein Bin Talal University, Jordan.

⁶ Center of Excellence in Environmental Studies, King Abdulaziz University, Jeddah, Saudi Arabia.

*E-mail: ismathassanali@gmail.com

Received: 9 May 2021 / Accepted: 14 June 2021 / Published: 30 June 2021

The current research aimed at investigating the potential corrosion inhibitory effect of essential oil extracted from *Moringa peregrina* leaves on carbon steel in acidic conditions. Gas chromatography (GC) and scanning electron microscope (SEM) were employed for studying the composition of the inhibitor and surface morphological changes of CS samples. Different experimental techniques such as chemical, electrochemical and surface characterization techniques were utilized for carbon steel (CS) immersed in 1.0 M HCl solution. Experimental observations suggest that through physical and chemical interactions, the inhibitor molecules form a stable layer on steel surface. The nature of adsorption of the investigated inhibitor onto the carbon steel surface obeyed the Langmuir isotherm model. Moreover, the electrochemical results revealed that the investigated inhibitor acts as a mixed-type inhibitor. Density function theory (DFT) calculations and molecular dynamic (MD) simulations were utilized to gain an insight into the possible interactions between the carbon steel surface and the inhibitor molecule mainly 9-Octadecadienoic acid (Z) present in the essential oil.

Keywords: Inhibition, Corrosion, *Moringa peregrina* Extract, Carbon Steel

1. INTRODUCTION

Iron and its alloys are frequently used in various industrial applications especially for infrastructure and transportation. These materials however are susceptible to degradation and deterioration in the form of corrosion which may be chemical, electrochemical or microbiological in nature. The severity of the corrosion damage will change depending on the nature of the environment with which the metal or the alloy is interacting. However, an acidic environment is known to be aggressive and eventually leads to accelerated corrosion of steel. Acids are commonly used in industries such as acid pickling, de-scaling, acid cleaning, desalination and petrochemical industries. In the extraction of crude oil process, steel structures are frequently exposed to hot acidic solutions [1]. However, the harsh conditions coupled with the corrosive nature of such acidic solutions subsequently leads to corrosion and deterioration of these steel structures. In order to protect metals and alloys against corrosion, corrosion inhibitors are frequently applied as chemicals dissolved in the acidic solution or incorporated into protective coatings. Corrosion inhibitors are known to inhibit corrosion as compared to the use of bare metals and alloys [2]. Various corrosion inhibitors such as organic inhibitors, vapour phase inhibitors, natural inhibitors have already been successfully applied and reported in literature. However, as low-cost and biodegradable materials, plant extracts as corrosion inhibitors are studied and reported by numerous researchers. These are also known as green inhibitors which may come as simple plant extracts or essential oils. The simple plant extracts include the use of orange peel extract [3], ethanol extract of *ocimum gratissimum* [4], leaf extract of *eribotiya japonica* thumb [5], gorse aqueous extract [6], peel garlic extract [7], *Acacia tortilis* leaves and barks extract [8], *Eucalyptus camaldulensis* seeds extract [9], ethanol extract of *Dialium guineense* leaves [10], ginko leaves extract [11], *irvingia gabonensis* extract [12], *Azadirachta indica* extract [13], *morus alba pendula* leaves extract [14], lemon balm extract [15], *pongamia pinnata* extract [16], fenugreek gum [17], gum Arabic [18], *Lannea coromandelica* leave extract [19], garlic extract [20], *Aloe vera* gel [21], sun flower seed hull extract [22], *Phyllanthus aramus* leaf extract [23], *saraca Ashoka* extract [24], algae *Cystoseira baccata* extract [25], *Uvaria chamea* root extract [26], *artemesia herba albamedium* plant extract [27], [28], *Glycyrrhiza glabra* leaves extract [29], *Eritriobotrya japonica* leaves extract [30], leaf extract of *Khaya senegalensis* (Mahogany) [31], leaves extract of *Cardiospermum halicababum* [32], *Rollinea occidentalis* extract [33], *Medicago sativa* plant extract [34], water hyacinth extract [35], *Cryptocaria nigra* extract [36], flavonoid extract of *Erigeron floribundus* [37], alkaloids extract of *Oxandra asbekii* plant [38], coffee husk [39]. The use of natural-green inhibitors for corrosion protection may be found in [40-44]. Corrosion inhibition by plant extracts in the form of essential oils has also been reported by many researchers. These include the essential oils of *croweacin* and *ammivisnaga lam* essential oil derivatives [45], combined admixture of essential oil extracts [46], essential oil of *saliva officinalis* [47], use of essential oil of *Artemisia mesatlantica* [48], essential oil of *Santolina pectinate* [49], cinnamon oil [50], acid garlic essential oils [51], *Thymus broussonnetii* essential oil [52], essential oil of *Eucalyptus globulus* [53], essential oil of master leaves of *Tetraclinis articulata* [54], fennel seeds essential oil [55], essential oils of *Alpinia galangal* [56], verbena essential oils [57] and the essential oil of *Thymus Sahraouian* [58]. Corrosion inhibition behaviour of various other essential oils may be found in [59] and [60].

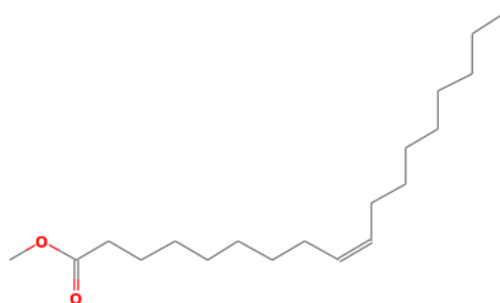
Almost all these extracts are being studied in acidic media such as HCl, H₂SO₄, HNO₃, and H₃PO₄ etc. for the corrosion inhibition of various types of steel. The corrosion inhibition characteristics of these plant extracts are mainly attributed to the presence of the complex organic compounds. Compounds that contain the hetero (polar) groups such as N, S, O are known as the adsorption centres due to the presence of pi or conjugated bonds or ring structures in their molecular structures.

The current research aims to explore and investigate the use of natural oil extract mainly containing 9-Octadecadienoic acid (Z) from *Moringa peregrina* leaves (OMPL) as corrosion inhibitor. To the best of our knowledge, no such research work has been conducted and this rarity prompted to report the case. The various types of interactions between the extracted inhibitor and steel surface in 1.0 M HCl solution are probed in the current research using chemical, electrochemical and surface studies.

2. EXPERIMENTAL

2.1. Extraction of inhibitor

The oil was extracted from leaves of *Moringa peregrina* plant using hexane as the solvent in the solvent extraction process. The extracted oil was analysed using GM-MS using a capillary column with dimensions Rtx-5ms-30m × 0.25 mm × 0.25 μm (GC/MS-QP2010-Ultra model, Shimadzu Company, Japan). Using the split mode, the oil sample was injected into the system in which helium was used as carrier gas and passed through the system with a flow rate of 1.61 ml/min and initial temperature of 60 °C, with step up rate of 10 °C/min, to final temperature of 300 °C, holding for 3 min. The temperatures of injection port, ion source and interface were kept at 300, 200 °C and 250 °C, respectively. The actual analysis was conducted for 26 min using the scan mode in the range of m/z 40-500 charges to ratio. The various components in the extracted oil were identified by matching mass fragmentation patterns and retention times with those available in the library, the National Institute of Standards and Technology (NIST), Cairo, Egypt. Scheme 1 represents the chemical structure of the main compound present in the extracted oil.



Scheme 1. Chemical structure of main chemical compound present in the extracted oil

2.2. Carbon steel samples and test solutions

The chemical compositions (wt. %) of the carbon steel (CS) samples were found to be around: C (0.36), Mn (0.66), Si (0.27), S (0.02), P (0.015), Cr (0.21), Mo (0.02), Cu (0.22), Al (0.06), and balance Fe. Using different grades of emery paper, the CS samples were abraded before being subjected to actual experimental conditions. The abraded CS samples were then rinsed thoroughly with distilled water followed by ethanol. With the help of distilled water, analytical grade hydrochloric acid was diluted to prepare the required concentrations of stock solutions.

2.3. Weight loss measurements

All experimental methods used in this study were based on the ASTM standards as reported earlier [61]. The carbon steel samples were immersed in both inhibited and uninhibited solutions for six hours at room temperature. CS samples were prepared according to the procedure stated earlier and each sample was weighted on a sensitive balance (± 0.1 mg). After each test, the CS samples were removed and thoroughly rinsed using distilled water and acetone and then dried and reweighted. All the tests were performed three times and their averaged values of the weight losses were used.

2.4. Electrochemical measurements

Electrochemical measurements were carried using Gamry Potentiostat (model 1000 interface) in a three-electrode conventional cell kit. The three-electrode cell kit consisted of a saturated (Ag/AgCl) electrode as a reference electrode (RE), carbon steel coupon surface having an exposed surface area of 0.28 cm^2 a working electrode (WE) that was immersed in the test solution and a platinum (Pt) auxiliary or counter electrode (CE). In order to attain equilibrium, the carbon steel sample was first immersed in the test solution for 30 minutes before conducting the actual electrochemical tests. This was followed by electrochemical impedance (EIS) measurements for which the impedance spectra were obtained within 100 kHz to 10 mHz frequency range and an AC amplitude of 5 mV. Potentiodynamic polarization (PDP) tests were conducted using scanning rate of 1 mV s^{-1} in the range from -800 to -200 mV. Linear polarization resistance (LPR) measurements were obtained at scanning rate of 0.125 mV/s in the range of -15mV to +15V. Further, the same sample was subjected to Electrochemical Frequency Modulation (EFM) technique using frequencies of 20 mHz and 50 mHz.

2.5. SEM studies

Scanning electron microscopy (SEM) was used to characterise the surface morphologies of the carbon steel samples with (2.0 g/L) and without the inhibitor. SEM analyses were carried out employing a Hitachi TM-1000 system with an accelerating voltage of 15 kV. The samples were analysed after 24 hrs of immersion time.

2.6. Theoretical evaluation

2.6.1. Quantum chemical details

In this study, the Conceptual Density Functional Theory (DFT) was utilized to get a better understanding of the essential oil extracted from leaves of *Moringa peregrina* during corrosion inhibition of steel. For this purpose, the geometry optimization and calculations of quantum chemical parameters of studied inhibitor were performed with the help of DMol3 as a reliable module integrated in the software (Materials Studio version 6.0) [62]. The generalized gradient first principles approximation (GGA) and Perdew, Burke and Ernzerhof formalism known as PBE with double numeric basis sets plus polarization (DNP) in the COSMO implicit solvent model were used for all calculations [63,64]. At the end of DFT analysis, the molecular structure of the investigated inhibitor was thoroughly examined and the optimized structure was then used to deduce some valuable derived data. Based on these calculations, the frontier molecular orbitals such as the energy of the highest occupied molecular orbital (E_{HOMO}) and energy of lowest unoccupied molecular orbital (E_{LUMO}) were estimated by applying the Koopmans' theorem [65, 66]. Moreover, in the light of HOMO and LUMO energies, the values of energy gap (ΔE), electronegativity, and the global hardness were also estimated. By applying Koopmans' theorem, the following equations can be obtained [67]:

$$IE = -E_{HOMO} \quad (1)$$

$$EA = -E_{LUMO} \quad (2)$$

$$\text{Absolute electronegativity} \quad \chi = \frac{IE+EA}{2} \quad (3)$$

$$\text{Absolute hardness} \quad \eta = \frac{IE-EA}{2} \quad (4)$$

$$\Delta E = E_{LUMO} - E_{HOMO} \quad (5)$$

In order to calculate the fraction of electrons transferred (ΔN), the Pearson method was used by applying the following equation [68, 69].

$$\Delta N = \frac{\phi - \chi_{inh}}{2(\eta_{Fe} - \eta_{inh})} \quad (6)$$

The work function (ϕ) of the Fe(110) is taken as 4.82 eV. Because $IE = EA$ for bulk metals, the hardness of iron is generally known as 0, [70, 71].

2.6.2. Molecular dynamic modeling

As a well-known tool, molecular dynamic (MD) simulations are being frequently utilized to assess the adsorption capacity of inhibitor molecules on metal surfaces. In fact, the intermolecular interactions between OMPL molecules and CS surfaces with respect to the functional properties of the inhibitor molecules have been subject to considerable discussions using MD simulations approach. In this study, MD modelling was performed using Forcite calculation, amorphous construction, and Build layer modules implemented in Material Studio program. Firstly, the Fe (110) surface with a slab of 5 Å was selected since it has a highly packed structure and associated with high stabilization energy. Secondly, MD simulations were carried out in a simulation box (25.28×25.28×38.32 Å³) which contained the main inhibitor in the form obtained OMPL oil and corrosive molecules and ions such as H₂O, Cl⁻ and H₃O⁺. MD simulations were achieved in the NVT canonical ensemble using an Anderson

thermostat, at the temperature of 298 K, time-step of 0.1 fs and a simulation time of 500 ps. For MD modelling, COMPASS force field (condensed phase optimized molecular potentials for atomistic simulation studies) was used for geometry optimization of molecular structure. In addition to the molecular structure geometry optimization, other useful information might be obtained by discussing the extent of adsorption with respect to the interactions of 9-Octadecadienoic acid (Z) as the main molecule of the extracted oil and the metal surface and binding energies of the system upon approaching equilibrium. The interaction and the binding energies ($E_{binding} = -E_{interaction}$) can be estimated using the following equation [72]:

$$E_{interaction} = E_{total} - (E_{surface+H_2O+H_3O^++Cl^-} + E_{inhibitor}) \quad (7)$$

3. RESULTS AND DISCUSSIONS

3.1. Phytochemical analysis

The chemical constituents of the extracted oil are obtained from Figure 1 and are listed in Table 1. The main constituent present in the extracted oil is 9-Octadecadienoic acid (Z) methyl ester as shown in Table 1.

Table 1. Chemical composition of the OMPL

Retention Time (min)	Area	Area in percentage (%)	Name of the substance
14.274	727845	0.21	Methyl tetradecanoate
15.410	121973	0.04	Pentadecanoic acid, methyl ester
16.247	811886	0.24	7-Hexadecenoic acid, methyl ester, (Z)
16.298	14516689	4.28	9-Hexadecenoic acid, methyl ester, (Z)
16.517	45405138	13.39	Hexadecanoic acid, methyl ester
17.312	733412	0.22	cis-10-Heptadecanoic acid, methyl ester
17.526	1371393	0.40	Heptadecanoic acid, methyl ester
18.255	1082757	0.32	9,12-Octadecadienoic acid (Z,Z) methyl ester
18.398	166848794	49.22	9-Octadecadienoic acid (Z) methyl ester
18.541	33258908	9.81	Methyl stearate
18.702	2513242	0.74	Oleic Acid
20.166	16223548	4.79	cis-13-Eicosenoic acid, methyl ester
20.217	1387305	0.41	cis-11-Eicosenoic acid, methyl ester
20.371	21046110	6.21	Eicosenoic acid, methyl ester
20.677	1336342	0.39	Tricyclo[20.8.0.0(7016)]triacontane
21.016	1495295	0.44	Oxiraneoctanoic acid, 3-octyl, methyl ester
21.230	400232	0.12	Heneicosanoic acid, methyl ester
22.076	22340099	6.59	Docosanoic acid, methyl ester
22.870	593999	0.18	Tricosanoic acid, methyl ester
23.645	6757981	1.99	Tetracosanoic acid, methyl ester
	338972948	100.00	

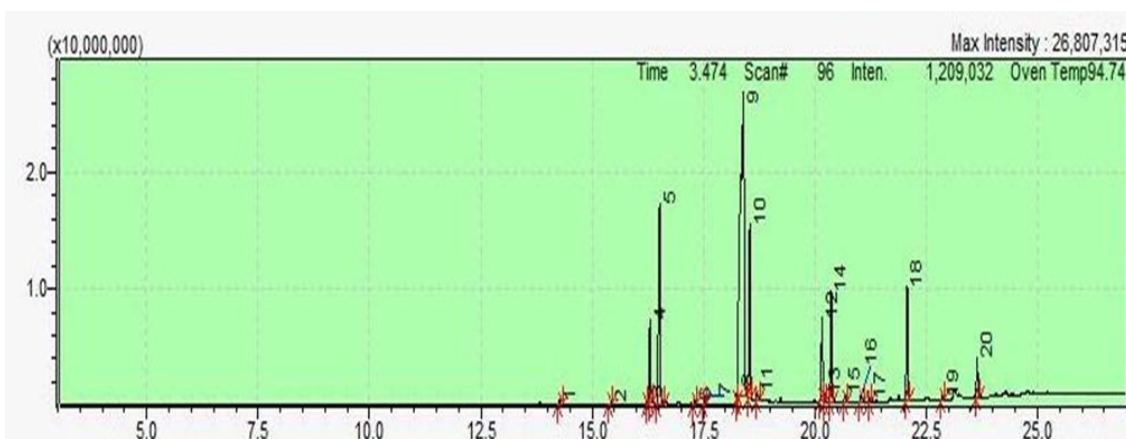


Figure 1. GC/MS spectrum for the natural oil extracted from leaves of *Moringa peregrina*

3.2. Weight loss measurements

The effect of different concentrations of OMPL inhibitor on the corrosion rate of carbon steel in 1.0 M HCl was evaluated using gravimetric tests. Equation (1) was used to determine the corrosion rate in millimetres per year (mm y^{-1}) as reported by [73]:

$$C_R = \frac{KW}{AT\rho} \tag{8}$$

where, K is a constant with a value of 8.76×10^4 , W is the mass loss (g), t is the time of exposure (h), A is the exposed area (cm^2) and ρ is the density of CS [74]. The corrosion inhibition efficiency, $\eta_{WL}(\%)$ of the investigated inhibitor can be calculated using the following equation [73]:

$$\eta_{WL}(\%) = \frac{C_R - C_R^\circ}{C_R} \times 100 \tag{9}$$

Where C_R and C_R° represent the corrosion rates in the presence and absence of the inhibitor derivatives, respectively.

Table 2. Weight loss parameters obtained for carbon steel in 1.0 M HCl solution containing different concentration of the extracted oil.

C(g/L)	Weight loss (mg)	C_R ($\text{mg cm}^{-2}\text{h}^{-1}$)	IE($\eta\%$)	Surface coverage (θ)
Blank	43.6	0.00156		
0.5	22.3	0.00080	49	0.49
1.0	20.5	0.00075	56	0.56
1.5	15.0	0.00054	66	0.66
2.0	14.0	0.00050	68	0.68

From the weight loss data tabulated in Table 2, high weight loss was observed for the blank CS sample in the acidic solution. However, the weight loss significantly decreased with the addition and subsequent increase in extracted oil concentration. As a result, the corrosion rate was observed to decrease while the corrosion inhibition efficiency increased with increasing the concentration of the

extracted oil. This behaviour is most likely due to the strong affinity of the inhibitor molecules to interact with iron atoms at higher inhibitor concentration (i.e. 9-Octadecadienoic acid (Z)) at which point the inhibitor molecules would enter the double layer level by replacing pre-existing water molecules [17,31,52,58]. The inhibitor demonstrated the maximum corrosion inhibition efficiency $\eta_{WL}(\%)$ of 68%, at 2.0 g/L.

3.3. Electrochemical studies

Electrochemical techniques are very robust and handy and are extensively used to obtain crucial information about the various interactions that might be occurring at the metal/inhibitor interface. Electrochemical studies are frequently conducted for metal samples subjected to corrosive conditions with and without the presence of inhibitors. Figure 2 shows the open circuit potential (OCP). It is clear that the potential reached almost constant values after about 1800 seconds.

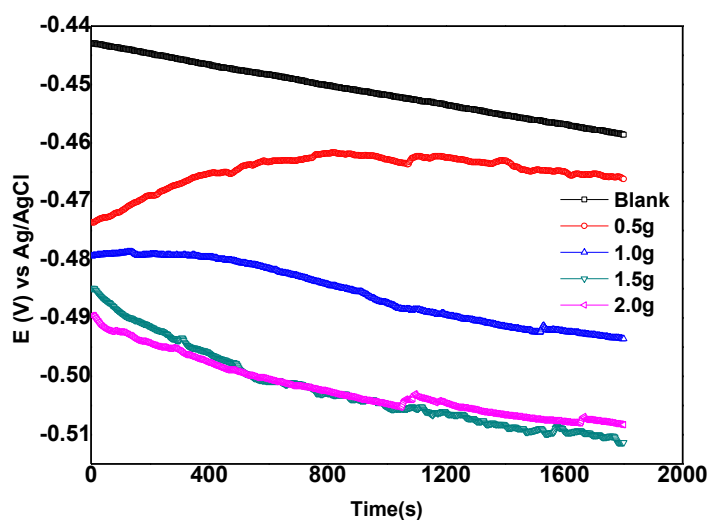


Figure 2. Variation of E_{OCP} vs. potential or reference electrode (Ag/AgCl) for CS electrode with and without inhibitor

Potentiodynamic polarization studies were conducted on the carbon steel samples immersed in 1.0M HCl solutions with different inhibitor concentrations and the obtained Tafel plots are shown in Figure 3. In order to calculate the corrosion potentials, the linear parts of Tafel curves were extrapolated and the results obtained are tabulated in Table 3.

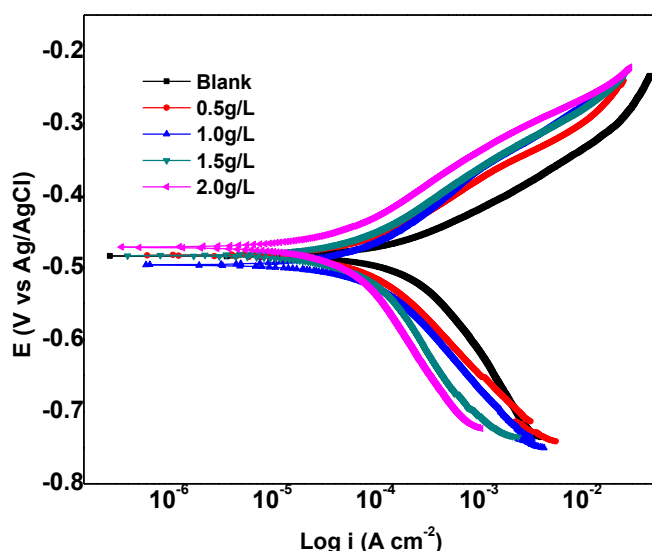


Figure 3. Potentiodynamic polarization curves for CS samples in 1.0 M HCl solution without inhibitor (blank) and with inhibitor (different concentrations) at room temperature

The corrosion inhibition efficiency ($\eta_{PDP}\%$) is calculated using equation (10) as reported by [73]:

$$\eta_{PDP}(\%) = \left[1 - \frac{i_{corr}}{i_{corr}^{\circ}} \right] \times 100 \tag{10}$$

where, i_{corr}° refers to the corrosion current density of the CS sample in uninhibited solutions, and i_{corr} is the corrosion current density in inhibited solution. Some key potentiodynamic kinetic parameters like corrosion current density (I_{corr}), corrosion potential (E_{corr}), anodic and cathodic Tafel slopes (β_a , β_c) and inhibition efficiencies are presented in Table 3.

Table 3. Potentiodynamic polarization parameters for CS samples in 1.0 M HCl solution without inhibitor (blank) and with inhibitor (different concentrations) at room temperature

C (g/L)	I_{corr} mA/cm ²	E_{corr} (mV vs Ag/AgCl)	Ba (mV/dec.)	Bc (mV/dec.)	Efficiency (η_{PDP}) %
Blank	202.00	-484	94	174	-
0.5	77.60	-483	91	136	61.6
1.0	91.30	-496	129	146	54.5
1.5	95.10	-483	130	231	53.0
2.0	43.30	-472	93	159	78.6

As expected, the current densities of both anodic and cathodic branches decreased by the addition of different concentrations of inhibitor. Because of the adsorption effect of the inhibitor molecules, the changes became more obvious as the concentration of the inhibitor increases, most likely due to the blocking of many of the active sites on the metal surfaces. Furthermore, the data revealed that the corrosion potential values were within close proximity to each other for the investigated inhibitor concentrations indicating that the inhibitor is a mixed type corrosion inhibitor [50,53]. This indicates that, the mechanism of the reaction remained unchanged whereas the available surface area for hydrogen evolution was considerably reduced and the access of hydrogen ions to the steel surface became more difficult [48,51]. Results from the polarization measurements are in good agreement with the weight loss measurements.

Electrochemical impedance spectroscopy (EIS) results are presented as Nyquist and Bode plots in Figures 4 and 6 respectively. Examination of the obtained results demonstrated that all Nyquist plots showed only one depressed capacitive semicircle and only one-time constant was detected in the Bode format. This further suggests that only one phenomenon happened, and the process of charge transfer is the only active way to control the dissolution of CS at solution/metal interface [75]. These results also reveal that the impedance response of the CS in the aggressive acidic medium was considerably influenced by the addition of the oil extracted inhibitor. As expected, the semicircles diameters were found to increase with increasing the concentrations of inhibitor.

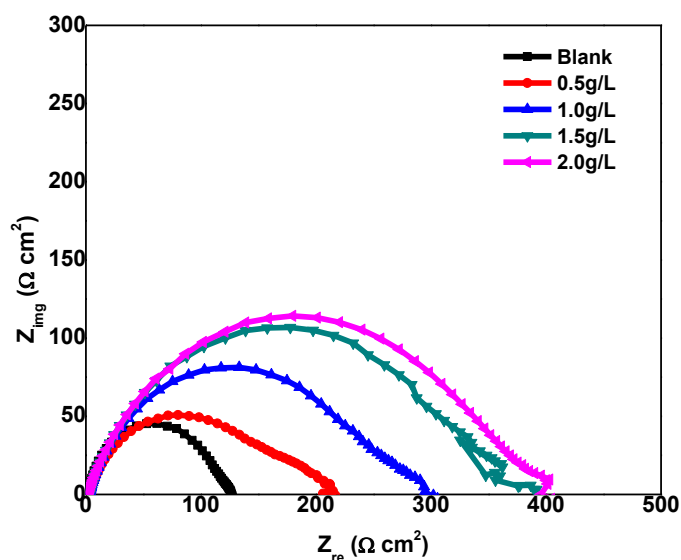


Figure 4. Nyquist plots for CS samples in 1.0 M HCl solution without inhibitor (blank) and with inhibitor (different concentrations) at room temperature

The EIS parameters obtained are listed in Table 4. It is important to note that an increase in the concentration of inhibitor results in more inhibitor molecules being adsorbed on the surface of CS samples, leading to formation of non-conducting protecting film [54] and reflected by the increase in charge transfer resistance, R_{ct} values. The R_{ct} value is a measure of the electron transfer across the

surface and is inversely proportional to corrosion rate so as the R_{ct} values increases as shown in Table 4, the corrosion rate is known to decrease.

All the electrochemical impedance parameters together with the inhibition efficiency $R_{p_{inh}}$ are given in Table 4. The inhibition efficiency was determined using equation (11):

$$\eta_{EIS}\% = \left[\frac{R_{p_{inh}} - R_p}{R_{p_{inh}}} \right] \times 100 \tag{11}$$

where, R_p and $R_{p_{inh}}$ refer to polarization resistances for CS samples in 1.0 M HCl solution without inhibitor (blank) and with inhibitor (different concentrations) at room temperature respectively.

Table 4. EIS parameters for carbon steel samples in 1M HCl solution without and with different concentrations of the extracted inhibitor at room temperature

C(g/L)	R_s ($\Omega\text{ cm}^2$)	R_{ct} ($k\Omega\text{ cm}^2$)	Goodness of fit $\chi^2 \times 10^{-3}$	$Y_0 \times 10^{-6}$	n	$\eta\%$
Blank	1.969	121.0	2.42	138.36	0.868	-----
0.5	3.059	186.5	5.78	137.6	0.718	35
1.0	2.726	267.0	3.106	122.7	0.750	55
1.5	3.021	345.3	2.665	88.40	0.751	65
2.0	3.116	369.7	4.412	38.23	0.780	68

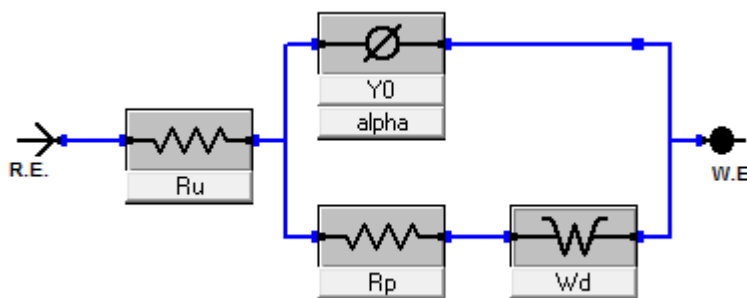


Figure 5. Equivalent circuit diagram used for the analysis of the electrochemical impedance spectroscopy data

The CPE formula most often used for adjustment and is shown in Figure 5. Moreover, the evolution of phase angle was addressed by measuring their values at randomly chosen frequency (1 kHz) (Figure 6). The value of phase angle increased significantly with the increase of inhibitor concentration. This designates more adsorption of inhibitor molecules which, in turn, leads to the formation of protecting film on CS surface. These results were further confirmed by increased absolute impedance at lower frequencies in the Bode plots. In addition, regardless of the concentrations used, the phase angle values were found higher than the blank sample, but lower than -90° , which describes

the non-ideal capacitor. The Nyquist diagrams presented in Figure 4 are depressed semicircles and not perfect as expected from the EIS theory. This phenomenon is common on solid electrodes. In general, a minor inclination of the impedance plots is commonly detected and usually is ascribed to the heterogeneity of CS [76]. Concurrently, a noticeable reduction in double layer capacitance was observed for the inhibited samples. This led to modifications in the CS-electrolyte interface and indicative of the better adsorption of the inhibitor on CS surface. As a result, a noticeable increase in the thickness of the dielectric double layer was observed that is suggestive of a minimum dissolution of steel.

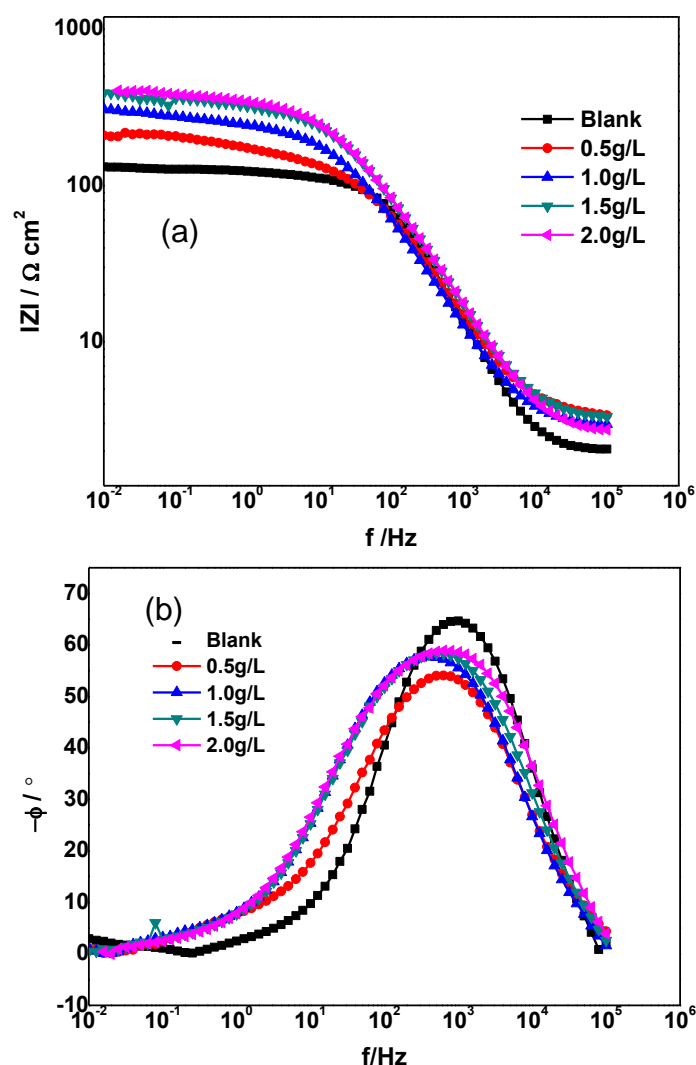


Figure 6. Bode (a) and phase angle (b) plots for carbon steel in 1M HCl solution containing different concentration of the inhibitor

Linear polarization resistance (LPR) is a rapid, non-destructive method commonly used in corrosion studies to gain corrosion rate. Table 5 shows data obtained from LPR experiments. It is obvious that the resistance increases and corrosion rate decreases with increasing the inhibitor

concentration. Results obtained from LPR experiments are in good agreement with those of the PDP and EIS experiments. Polarisation resistance values obtained from the LPR are much higher for the inhibited samples than that of the uninhibited samples as tabulated in (Table 5), pointing to a decrease in CS dissolution reaction in the acidic solutions.

Table 5. Linear Polarization Resistance (LPR) parameters for uninhibited and inhibited CS samples in 1.0 M HCl solution with various inhibitor concentration at 25 °C, with β_a and $\beta_c = 120 \times 10^{-3}$ mV/dec.

C(g/L)	L fit (mV)	U fit (mV)	I_{corr} mA/cm ²	E_{corr} (mV Vs Ag/AgCl)	Rp (ohms)	Corrosion Rate (mpy)
Blank	-486	-476	173	-482	150	619
0.5	-497	-483	106	-490	246	378
1.0	-503	-495	86	-499	303	307
1.5	-525	-514	66	-520	395	235
2.0	-493	-485	70	-484	370	251

Further, electrochemical frequency modulation (EFM) was also used to determine the corrosion rate. Corrosion parameters for uninhibited and inhibited CS samples in 1M HCl solution with various inhibitor concentrations at 25 °C are presented in Table 6. The EFM method has the benefit that the corrosion rate can be determined without previous knowledge of the Tafel constants. The corrosion rates attained from the EFM measurements are showed in Table 6. The EFM measurements also provide an internal self-check in the form of the two EFM Factors viz. F2 and F3. These two factors should have approximately the values 2.0 and 3.0, respectively if all of the conditions of EFM theory have been met. Table 4 proves that all values of F2 and F3 are approximately 2 and 3 respectively.

Table 6. Electrochemical Frequency Modulation (EFM) parameters for uninhibited and inhibited CS samples in 1M HCl solution with various inhibitor concentrations at 25 °C,

C(g/L)	I_{corr} mA/cm ²	$\beta 1$ (10 ⁻³)	$\beta 2$ (10 ⁻³)	Corrosion Rate (mpy)	F2	F3
Blank	0.1527	99.68	112.1	544.9	2.152	3.173
0.5	0.1477	129.0	135.2	527.2	1.844	3.247
1.0	0.1454	152.3	170.8	519.1	1.644	2.804
1.5	0.1129	148.0	178.2	402.9	1.965	3.347
2.0	0.0868	107.9	118.5	310.1	1.771	2.925

3.4. Adsorption isotherm

Many published studies on natural products used as corrosion inhibitors on steel surfaces have concluded that the corrosion inhibition by the inhibitor molecules is achieved mainly by adsorption

onto the metal surfaces. The type of adsorption may be physical, chemical or physicochemical in nature. The actual nature of adsorption may be deduced by utilization of appropriate adsorption isotherm models [76]. The experimental data in the current investigation were modelled using different adsorption isotherms including Langmuir, Frumkin and Temkin. The Langmuir model best fitted the experimental data and gave the best explanation of the investigated inhibitor adsorption process. The linear equation of this model is [77]:

$$\frac{C_{\text{inh}}}{\theta} = \frac{1}{K_{\text{ads}}} + C_{\text{inh}} \quad (12)$$

Where C_{inh} represents the inhibitor concentration and K_{ads} is the adsorption-desorption equilibrium constant. The $\Delta G_{\text{ads}}^{\circ}$ values (free energy change) were determined using equation 13:

$$\Delta G_{\text{ads}}^{\circ} = -RT \ln(K_{\text{ads}} \times 55.5) \quad (13)$$

Where, R represents the universal gas constant (8.3144598 J/K), T is absolute temperature and the value of 55.5 is the concentration of H_2O in solution in mol L^{-1} .

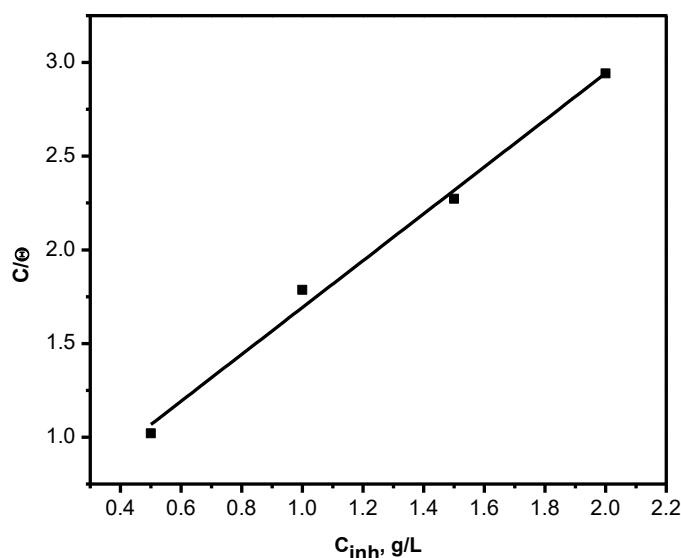


Figure 7. Plot of Langmuir adsorption model fitted experimental data from EIS for CS in 1M HCl containing different concentrations of the inhibitor

The plot of C_{inh}/θ vs C_{inh} yield the best fit as shown in Figure 7 with R^2 and slope values close to 1 leading to the conclusion that the adsorption of studied inhibitor on the CS surface follows the Langmuir isotherm model. Values of free energy change and the adsorption-desorption equilibrium constant were determined as 12.0 kJ/mole and 2.26 respectively. These results are indicative of spontaneous adsorption process. These results also revealed that since the adsorption free energy value of the tested inhibitor is less than -20 kJ mol^{-1} , the adsorption nature of the inhibitor on CS surface can be confirmed as physical adsorption [78].

3.5. SEM study

SEM investigations were conducted and the obtained pictures of the CS before and after soaking in 1.0 M HCl are presented in Figure 8. Figure 8a shows a highly damaged and corroded steel surface mostly because of the rapid corrosion attack in acidic solution. However, smoother surface morphology was observed as shown in Figure 8b after the addition of OMPL inhibitor into the acid solution. This behaviour is mainly attributed to the formation of an adsorption layer on the steel surface thus reducing the severity of corrosion. However, there are few minor scratches and visible polishing lines which are most likely the residue of the steel surface preparation and pre-treatment processes prior to the actual immersion testing and may also be due to moderate efficiency of the inhibitor.

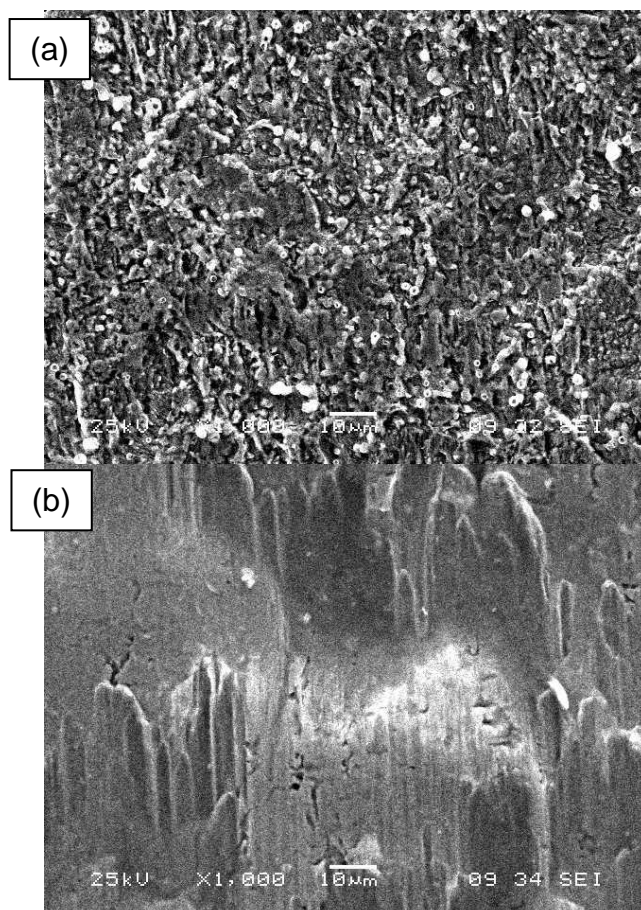


Figure 8. SEM images for (a) surface of CS immersed in 1M HCl solution without inhibitor and (b) surface of carbon inhibited by 2.0 ppm concentration of the inhibitor

3.6. DFT calculation

Much of our knowledge of DFT methods in corrosion science is based on theoretical concepts that study the relationship between inhibitory structures and their inhibition properties. Frontier orbital

energies, chemical reactivity descriptors (for example, and electron transfer fraction, electronegativity, electron affinity and ionization energy,) could arguably provide essential evidences on the inhibition performance of inorganic and organic molecules against corrosion of metals and alloys. This work has been carried out in the liquid phase and the optimized molecular structure; HOMO and LUMO of the studied compound are presented graphically in Figure 9. From this Figure, we can see that the distribution of the HOMO orbital is around of some carbon atoms as well as double bond part in the molecular structure of 9-Octadecadienoic acid (Z).

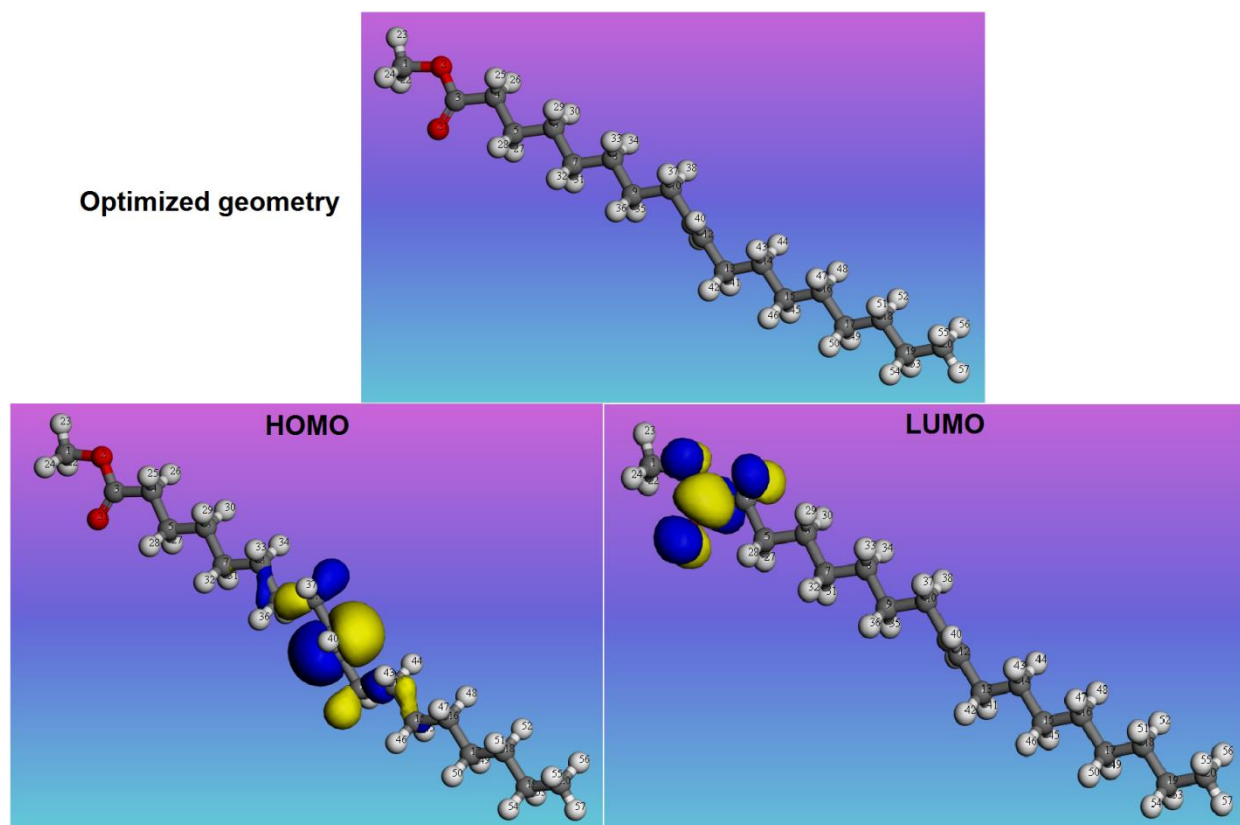


Figure 9. Optimized geometry, LUMO and HOMO orbitals obtained using DFT method for 9-Octadecadienoic acid (Z) inhibitor

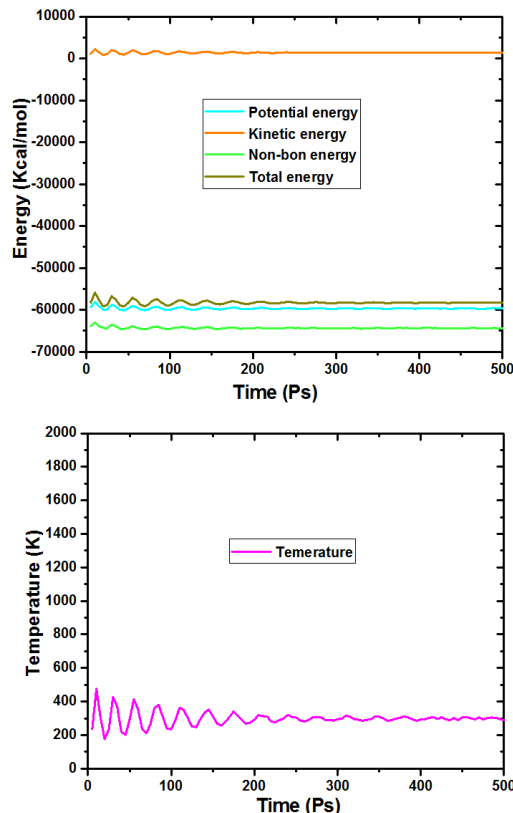
In contrast, the electron density of LUMO is concentrated around the methyl acetate group. Therefore, it can be concluded that the double bond and adsorption centers such as methoxy group and lone pair of oxygen atom can perfectly facilitate the donor-acceptor interaction between metal surface and inhibitor molecule. In addition, some of the quantum chemical descriptors such as E_{HOMO} , E_{LUMO} and ΔN_{110} are listed in Table 7. It is well-known that any molecule having high HOMO energy value will be effective in terms of the prevention of the corrosion of metals surfaces. On the other hand, low LUMO energy value shows that the molecule is a good electron acceptor. Energy gap is also a closely related parameter [12–14].

Table 7. The quantum chemical parameters for OMPL inhibitor (mainly 9-Octadecadienoic acid (Z)) analysed from DFT method in aqueous solution.

Molécule	E_{HOMO} (eV)	E_{LUMO} (eV)	ΔE_{gap} (eV)	EA(eV)	IE(eV)	χ (eV)	ΔN_{110}
OMPL	-4.956	-1.142	3.814	4.956	1.142	3.049	0.464

It is important to note that many of plant extract has been the subject of many classic studies in the corrosion inhibition science, but a search of the literature revealed few studies which investigate the key role of these inhibitor molecules based on quantum chemical parameters calculated by using DFT approach. Most importantly, we would not have been able to discuss these reactivity parameters without comparing them with those of similar inhibitors. Further, as can be understood from the information given in Table 7, the energy gap of 9-Octadecadienoic acid (Z) molecule is low, suggesting that the chemical reactivity of the inhibitor under study is important and it's an indicator of its efficiency against the corrosion of carbon steel. Additionally, the estimated value of transferred electrons (ΔN_{110}) of 9-Octadecadienoic acid (Z) molecule is positive confirming that this inhibitor is a good electron donor. Finally, it is clear that the application of DFT is very important to predict the inhibition performances of 9-Octadecadienoic acid (Z) molecule against the corrosion of metal surface.

3.7. MD Simulation

**Figure 10.** Temperature and energy equilibrium curves of the 9-Octadecadienoic acid (Z) compound adsorbed on the iron surface in solution.

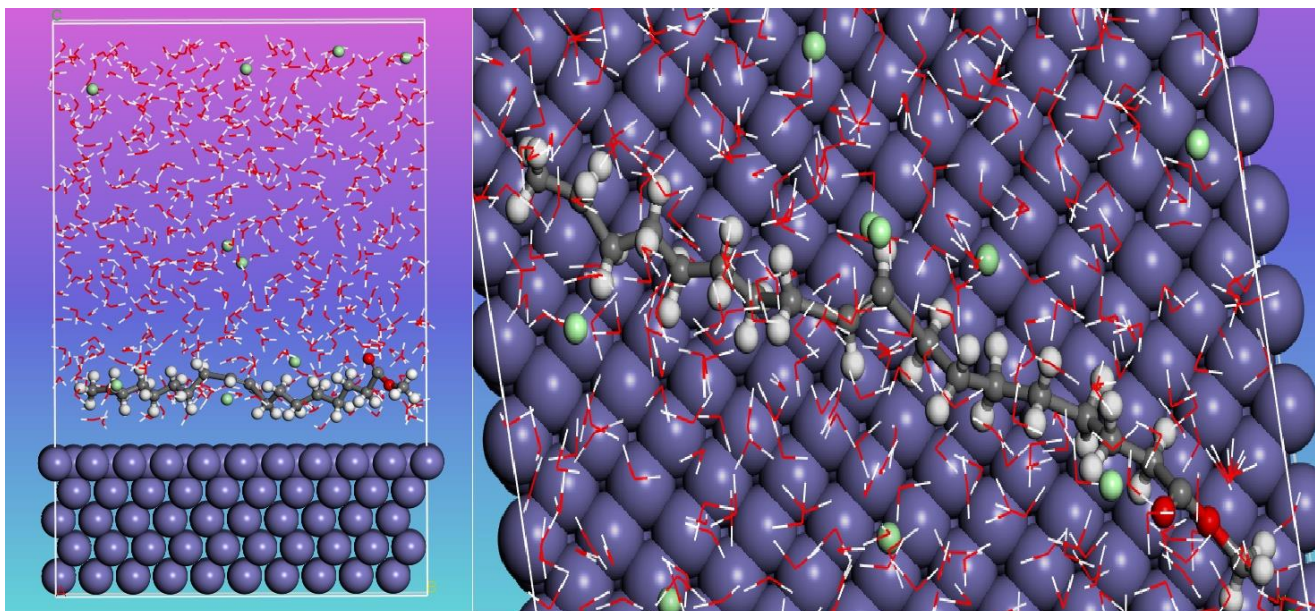


Figure 11. Side and top views of the most appropriate configuration for adsorption of 9-Octadecadienoic acid (Z) compound on Fe (110) surface calculated using MD simulations in the aqueous solution at 298 K.

Evidence suggests that the adsorption mechanism is among the most important factors that influence the efficiency of inhibitors on metal surfaces. In fact, MD simulation is a key strategy for determining the effect of active sites responsible for inhibitor-metal interactions. In this investigation, MD simulations give more confirmation to the results obtained by DFT calculations and the experimental data. The MD modeling was performed in the liquid solution for assessing the 9-Octadecadienoic acid (Z) inhibitor activity on the surface of iron. As mentioned earlier in experimental part to this paper, the simulations were performed under NVT conditions in which the equilibrium state was mostly maintained for the studied system (Figure 10). At optimized conditions, Figure 11 provides the final adsorption configurations of 9-Octadecadienoic acid (Z) molecules adsorbed on the Fe (110). From the data in Figure 11, it is apparent that the adsorption of 9-Octadecadienoic acid (Z) molecule on the iron surface is almost parallel, and it is adsorbed with a planar arrangement that can help ensure coverage of a maximum surface area of the surface, thus preventing the surface from corrosion. It is obvious from Figure 11 that adsorption of 9-Octadecadienoic acid (Z) molecules on the iron surface is almost parallel. Moreover, the molecules were adsorbed in planar configuration that helps to cover maximum surface area, resulting in higher corrosion protection efficiency. In fact, the degree of interaction by parallel arrangement of 9-Octadecadienoic acid (Z) molecules on the iron surface is mostly affected by the length of the molecular structure as well as the active sites present in the investigated compound. These results may be explained and more understood by interpreting the interaction and binding energies estimated by MD simulations. The higher interaction energy reflects the strong adsorption between an inhibitor compound and iron surface as in agreement with other published work [79, 80]. The results, as evaluated by MD simulations, indicate that the 9-Octadecadienoic acid (Z) inhibitor showed a strong interaction and bending affinity towards the iron

surface in which $E_{\text{interaction}}$ value equal to $-532.86 \text{ kJ mol}^{-1}$ ($E_{\text{binding}} = 532.86 \text{ kJ mol}^{-1}$). In addition, higher binding energies suggest that the 9-Octadecadienoic acid (Z) was adsorbed with the aid of more than one reactive center [81–83]. These factors may explain the relatively good adsorption efficiency between the 9-Octadecadienoic acid (Z) inhibitor and iron surface. All such findings support evidence from experimental and DFT observations obtained in this investigation, which showed that 9-Octadecadienoic acid (Z) compound showed a strong anti-corrosion efficiency for CS under acidic conditions.

3.8. Anticorrosion mechanism of 9-Octadecadienoic acid (Z) (main compound of OMPL)

Generally, the anticorrosion and protection mechanisms of essential oils are known to provide protection in three possible ways depending on action mode. These include; 1) geometric blocking effect where the inhibition is achieved by a reduction in reaction site size on metal surface, 2) active site blocking effect, and 3) the electrocatalytic effect.

In the last two cases, inhibition possibly occurs because of changes in the average activation energy boundaries of the cathodic and anodic corrosion reactions [59]. Through the adsorption process, both the cathodic and anodic reactions on the CS surface are suppressed by essential oils. Many studies have been published on the biological properties of OMPL, however, no comprehensive study on the efficiency and mechanism of 9-Octadecadienoic acid (Z) compound present in the OMPL as a corrosion inhibitor is found. Hence, the purpose of the current study is to underpin the potential of the 9-Octadecadienoic acid (Z) compound for corrosion inhibition. Results from the current investigation reveal that 9-Octadecadienoic acid (Z) (main compound present in OMPL) is an effective corrosion inhibitor with great electronic properties. It is believed that the studied inhibitor has a greater proton affinity because of the existence of heteroatoms in its molecular structure. The same feature has been reported in many studies on corrosion inhibition under acidic conditions [78]. Overall, corrosion inhibition efficiencies obtained from weight loss, PDP curves and EIS are in good agreement.

4. CONCLUSION

The corrosion inhibition effect of 9-Octadecadienoic acid (Z) which is the main compound in the natural oil extracted from leaves of *Moringa peregrina* (OMPL) on the corrosion behaviour of CS in 1.0 M HCl solution has been presented in this study. The corrosion inhibition mechanisms were probed to demonstrate the efficiency of this inhibitor through experiments. The investigated inhibitor exhibited good inhibitive performances as compared with the other similar compounds. Electrochemical results revealed mixed type inhibiting behaviour for the tested inhibitor. Adding the inhibitor to the acid test solutions resulted in increased polarization resistance and subsequently decreased the double-layer capacitance values. A detailed computational study of factors potentially affecting the efficiency of the investigated inhibitor is also reported in this work. Again, theoretical results demonstrated a strong and consistent association with experimental findings.

CONFLICT OF INTEREST

“The authors of this manuscript have no conflict of interest to declare.”

ACKNOWLEDGEMENTS

The authors extend their appreciation to the Deanship of Scientific Research at King Khalid University for funding this work through research groups program under grant number R.G.P.1/196/41.

References

1. V. Saini, H. Kumar, DAA, *Int. Lett. Chem. Phys. Astron.*, 36 (2014) 174.
2. T. Hu, H. Shi, T. Wei, F. Liu, S. Fan, E.H. Han, *Corros. Sci.*, 95 (2015) 152.
3. N. M'hiri, D. Veys-Renaux, E. Rocca, I. Ioannou, N.M. Boudhrioua, M. Ghoul, *Corros. Sci.*, 102 (2016) 55.
4. N.O. Eddy, S.A. Odoemelam, I.N. Ama, *Green Chem. Lett. Rev.*, 3 (2010) 165.
5. W. Yang, Q. Wang, K. Xu, Y. Yin, H. Bao, X. Li, L. Niu, S. Chen, *Materials*, 10 (2017) 956.
6. R. da S. Trindade, M.R. Dos Santos, R.F.B. Cordeiro, E. D'Elia, *Green Chem. Lett. Rev.*, 10 (2017) 444.
7. L.S. Barreto, M.S. Tokumoto, I.C. Guedes, H.G. De Melo, F.D.R. Amado, V.R. *Rev. Mater.*, 22 (2017).
8. I. H. Ali, A. M. Idris, M. H. A. Suliman, *Int. J. Electrochem. Sci.*, 14 (2019) 6406.
9. I.Y. Lawan, F.K. Abdullah, S. Idris, S.D. Yamta, A. Hudu, *Earthline J. Chem. Sci.*, 3 (2020) 61.
10. S.E. Adeniji, B.A. Akindehinde, *J. Electrochem. Sci. Eng.*, 8 (2018) 219.
11. S. Deng, X. Li, *Corros. Sci.* 55 (2012) 407.
12. C.C. Onah, C.N. Mbah, K.C. Nnakwo, *Am. J. Chem. Mater. Sci.*, 6 (2019) 15.
13. S.K. Sharma, A. Peter, I.B. Obot, *J. Anal. Sci. Technol.*, 6 (2015).
14. M. Jokar, T.S. Farahani, B. Ramezanzadeh, *J. Taiwan Inst. Chem. Eng.*, 63 (2016) 436.
15. N. Asadi, M. Ramezanzadeh, G. Bahlakeh, B. Ramezanzadeh, *J. Taiwan Inst. Chem. Eng.*, 95 (2019) 252.
16. T.K. Bhuvanewari, V.S. Vasantha, C. Jeyaprabha, *Silicon*, 10 (2018) 1793.
17. H. Lgaz, I.-M. Chung, R. Salghi, I.H. Ali, A. Chaouiki, Y. El Aoufir, M.I. Khan, *Appl. Surf. Sci.*, 463 (2019) 647.
18. K. Azzaoui, E. Mejdoubi, S. Jodeh, A. Lamhamdi, E. Rodriguez-Castellón, M. Algarra, A. Zarrouk, A. Errich, R. Salghi, H. Lgaz, *Corros. Sci.*, 129 (2017) 70.
19. P. Muthukrishnan, B. Jeyaprabha, P. Prakash, *Arab. J. Chem.*, 10 (2017) 2343.
20. M.P. Asfia, M. Rezaei, G. Bahlakeh, *J. Mol. Liq.*, 315 (2020) 113679.
21. A.K. Singh, S. Mohapatra, B. Pani, *J. Ind. Eng. Chem.*, 33 (2016) 288.
22. H. Hassannejad, A. Nouri, *J. Mol. Liq.*, 254 (2018) 377.
23. K.K. Anupama, K. Ramya, A. Joseph, *J. Mol. Liq.*, 216 (2016) 146.
24. A. Saxena, D. Prasad, R. Haldhar, G. Singh, A. Kumar, *J. Mol. Liq.*, 258 (2018) 89.
25. T. Benabbouha, R. Nmila, M. Siniti, K. Chefira, H. El Attari, H. Rchid, *SN Appl. Sci.*, 2 (2020) 662.
26. L. Nnanna, O. Nwadiuko, F. O. Nwosu, D. O. Dimoji, K. I. Mejeh, *Afr. J. Pure Appl. Chem.*, 7 (2013) 302.
27. M. Boudalia, R.M. Fernández-Domene, M. Tabyaoui, A. Bellaouchou, A. Guenbour, J. García-Antón, *J. Mater. Res. Technol.*, 8 (2019) 5763.
28. A. Berrissoul, E. Loukili, N. Mechbal, F. Benhiba, A. Guenbour, B. Dikici, A. Zarrouk, A. Dafali, *J. Colloid Interface Sci.*, 580 (2020) 740.
29. E. Alibakhshi, M. Ramezanzadeh, G. Bahlakeh, B. Ramezanzadeh, M. Mahdavian, M. Motamedi, *J. Mol. Liq.*, 255 (2018) 185.
30. X. Zheng, M. Gong, Q. Li, L. Guo, *Sci. Rep.*, 8 (2018) 1.

31. I. H. Ali, *Int. J. Electrochem. Sci.*, 11 (2016) 2130.
32. I. Y. Suleiman, A. Kasim, S. R. Ochu, *J. Bio- Tribo- Corros.*, 5, (2019) 65.
33. P.E. Alvarez, M.V. Fiori-Bimbi, A. Neske, S.A. Brandán, C.A. Gervasi, *J. Ind. Eng. Chem.* 58 (2018) 92.
34. A.M. Al-Turkustani, S.T. Arab, L.S.S. Al-Qarni, *J. Saudi Chem. Soc.*, 15 (2011) 73.
35. O. Babatunde, S. O. Ogunrinde, D. S. Aribike, A. A. Adeyemi, *J. Material. Sci. Eng.*, (2020) 5.
36. M. Faiz, A. Zahari, K. Awang, H. Hussin, *RSC Adv.*, 10 (2020) 6547.
37. F.E. Abeng, V.D. Idim, 98 (2018) 89.
38. M. Lebrini, F. Robert, A. Lecante, C. Roos, *Corros. Sci.*, 53 (2011) 687.
39. R.F.B. Cordeiro, A.J.S. Belati, D. Perrone, E. D'Elia, *Int. J. Electrochem. Sci.*, 13 (2018) 12188.
40. B. HongyuWei, L. Heidarshenas, G. Zhou, Q. Hussain, K. Li, (Ken) Ostrikov, *Mater. Today Sustainability*, 10 (2020) 100044.
41. S.A. Umoren, M.M. Solomon, I.B. Obot, R.K. Suleiman, *J. Ind. Eng. Chem.*, 76 (2019) 91.
42. C. Verma, E.E. Ebenso, I. Bahadur, M.A. Quraishi, *J. Mol. Liq.*, 266 (2018) 577.
43. S.K. Sharma, E. Khamis, *J. Corros. Sci. Eng.*, 11 (2008) 1.
44. B.E.A. Rani, B.B.J. Basu, *Int. J. Corros.*, 12 (2012) 15.
45. A. Chraka, I. Raissouni, N. Ben Seddik, S. Khayar, S. El Amrani, M. El Hadri, F. Chaouket, D. Bouchta, *Mediterr. J. Chem.*, 10 (2020) 378.
46. R.T. Loto, O. Olowoyo, *S. Afr. J. Chem. Eng.*, 26 (2018) 35.
47. H. Bourazmi, M. Rbaa, R. Benkaddour, F. Bentiss, C. Jama, J. Costa, M. Tabyaoui, A. Zarrouk, *Prot. Met. Phys. Chem*, 56 (2020) 438.
48. K. Boumhara, F. Bentiss, M. Tabyaoui, J. Costa, J.M. Desjobert, A. Bellaouchou, A. Guenbour, B. Hammouti, S.S. Al-Deyab, *Int. J. Electrochem. Sci.*, 9 (2014) 1187.
49. M. Manssouri, A. Laghchimi, A. Ansari, M. Znini, Z. Lakbaibi, Y. El Ouadi, L. Majidi, *Mediterr. J. Chem.*, 10 (2020) 253.
50. M.M. Bouraoui, S. Chettouh, T. Chouchane, N. Khellaf, *J. Bio- Tribo-Corros.*, 5 (2019) 1.
51. L. Afia, O. Benali, R. Salghi, E.E. Ebenso, S. Jodeh, M. Zougagh, B. Hammouti, *Int. J. Electrochem. Sci.*, 9 (2014) 8392.
52. H. Chebli, M. Zaafrani, A. Batah, M. Berrabah, A. Mziouid, N. Heimeur, B. Chebli, R. Salghi, *J. Bio- Tribo-Corros.*, 5 (2019) 1–10.
53. S. Rekkab, H. Zarrok, R. Salghi, A. Zarrouk, L. Bazzi, B. Hammouti, Z. Kabouche, R. Touzani, M. Zougagh, *J. Mater. Environ. Sci.*, 3 (2012) 613.
54. A. Djouahri, S. Sebiane, F. Kellou, L. Lamari, N. Sabaou, A. Baaliouamer, L. Boudarene, *J. Essent. Oil Res.*, 29 (2017) 169.
55. N. Lahhit, A. Bouyanzer, J.M. Desjobert, B. Hammouti, R. Salghi, J. Costa, C. Jama, F. Bentiss, L. Majidi, *Port. Electrochim. Acta*, 29 (2011) 127.
56. S.O. Ajeigbe, N. Basar, M.A. Hassan, M. Aziz, *ARPN J. Eng. Appl. Sci.*, 12 (2017) 2763.
57. D. Ben Hmamou, R. Salghi, A. Zarrouk, H. Zarrouk, M. Errami, B. Hammouti, L. Afia, L. Bazzi, L. Bazzi, *Res. Chem. Intermed.*, 39 (2013) 973.
58. Z. Bensouda, M. Driouch, R.A. Belakhmima, M. Sfaira, M. Ebn Touhami, A. Farah, *Port. Electrochim. Acta*, 36 (2018) 339.
59. S.M.Z. Hossain, S.A. Razzak, M.M. Hossain, *Arabian J. Sci. Eng.*, 45 (2020) 7137.
60. M. Abdullah Dar, *Ind. Lubr. Tribol.*, 63 (2011) 227.
61. M. Chafiq, A. Chaouiki, M. Damej, H. Lgaz, R. Salghi, I. H. Ali, M. Benmessaoud, S. Masroor, I-M. Chung, *J. Mol. Liq.*, 309 (2020) 113070.
62. Materials Studio, Revision 6.0, (2013).
63. B. Delley, *J. Chem. Phys.*, 113 (2000) 7756.
64. J.P. Perdew, K. Burke, M. Ernzerhof, *Phys. Rev. Lett.*, 77 (1996) 3865.
65. A. Kokalj, *Electrochim. Acta*, 56 (2010) 745.
66. M.J. Dewar, W. Thiel, *J. Am. Chem. Soc.*, 99 (1977) 4899.

67. R.G. Pearson, *Proc. Natl. Acad. Sci.*, 83 (1986) 8440.
68. B. Gómez, N.V. Likhanova, M.A. Dominguez Aguilar, O. Olivares, J.M. Hallen, J.M. Martínez-Magadán, *J. Phys. Chem. A.*, 109 (2005) 8950.
69. N. Kovačević, A. Kokalj, *Corros. Sci.*, 53 (2011) 909.
70. R.G. Pearson, *Inorg. Chem.*, 27 (1988) 734.
71. A. Kokalj, *Chem. Phys.*, 393 (2012) 1.
72. V. Sastri, J. Perumareddi, *Corrosion*, 53 (1997) 617.
73. L. Li, X. Zhang, J. Lei, J. He, S. Zhang, F. Pan, *Corros. Sci.*, 63 (2012) 82.
74. S.S. de Assunção Araújo Pereira, M.M. Pêgas, T.L. Fernández, M. Magalhães, T.G. Schöntag, D.C. Lago, L.F. de Senna, E. D'Elia, *Corros. Sci.*, 65 (2012) 360.
75. D. Ben Hmamou, R. Salghi, A. Zarrouk, H. Zarrouk, M. Errami, B. Hammouti, L. Afia, L. Bazzi, L. Bazzi, *Res. Chem. Intermed.*, 39 (2013) 973.
76. M.A. Deyab, M.M. Osman, A.E. Elkholy, F. El-Taib Heakal, *RSC Adv.*, 7 (2017) 45241.
77. A. Singh, K.R. Ansari, J. Haque, P. Dohare, H. Lgaz, R. Salghi, M.A. Quraishi, *J. Taiwan Inst. Chem. Eng.*, 82 (2018) 233.
78. L.O. Olasunkanmi, I.B. Obot, E.E. Ebenso, *RSC Adv.*, 6 (2016) 86782.
79. E. Ech-chihbi, A. Nahlé, R. Salim, F. Benhiba, A. Moussaif, F. El-Hajjaji, H. Oudda, A. Guenbour, M. Taleb, I. Warad, *J. Alloys Compd.*, (2020) 155842.
80. A. Chaouiki, H. Lgaz, S. Zehra, R. Salghi, I.-M. Chung, Y. El Aoufir, K.S. Bhat, I.H. Ali, S.L. Gaonkar, M.I. Khan, *J. Adhes. Sci. Technol.*, 33 (2019) 921.
81. A. Chaouiki, H. Lgaz, R. Salghi, M. Chafiq, H. Oudda, K. Bhat, I. Cretescu, I. Ali, R. Marzouki, I. Chung, *Colloids Surf., A* 588 (2020) 124366.
82. H. Lgaz, R. Salghi, A. Chaouiki, Shubhalaxmi, S. Jodeh, K. Subrahmanya Bhat, *Cogent Eng.*, 5 (2018) 1441585.
83. P. Dohare, M. Quraishi, C. Verma, H. Lgaz, R. Salghi, E. Ebenso, *Results Phys.*, 13 (2019) 102344.